RESEARCH PAPER

Micro-channel flow boiling heat transfer of R-134a, R-236fa, and R-245fa

Lorenzo Consolini · John R. Thome

Abstract The rapid development of micro-thermal technologies has conveyed an increasing interest on convective boiling in micro-channels. Although there is general agreement that these systems may be able to dissipate potentially very high heat fluxes per unit volume, their heat transfer characteristics are still unclear and require investigation. The present study illustrates heat transfer data for flow boiling in a single micro-channel, for two channel diameters, namely, 510 and 790 μm, three fluids, namely, R-134a, R-236fa and R-245fa, mass velocities from 300 to 2,000 kg/m^2 s, and heat fluxes up to 200 kW/m^2. Stable flow boiling heat transfer data are analyzed through a parametric investigation, and are also confronted with measurements in the presence of two-phase oscillatory instabilities, which were found to significantly change the trends with respect to vapor quality.

Keywords Micro-channel · Flow boiling · Heat transfer · Oscillatory instability

1 Introduction

Since the early 1980s, the growing need of industry for compact, high heat flux cooling devices has elevated the interest in understanding the mechanisms and potential of convective boiling in small-size channels to a "global" level. From the experience developed on conventional heat

L. Consolini · J. R. Thome (✉)
Laboratoire de Transfert de Chaleur et de Masse (LTCM),
Faculté de Sciences et Techniques de l'Ingénieur (STI),
École Polytechnique Fédérale de Lausanne (EPFL),
1015 Lausanne, Switzerland
e-mail: john.thome@epfl.ch

sinks, a two-phase flow in a micro-channel is expected to present several important benefits when compared to other competing methods for thermal control. Convective boiling often combines high heat transfer at low mass flow rates as well as a nearly constant channel wall and fluid temperature due to the thermally saturated nature of a liquid–vapor mixture. The initial purpose of the studies on two-phase heat transfer in micro-channels was (and still is, to a certain extent) aimed at understanding the mechanisms controlling the flow boiling process. Lazarek and Black (1982) reported experimental heat transfer coefficients for flow boiling of R-113 in a vertical tube with an inner diameter of 3.1 mm. Their heat transfer coefficients showed a strong dependency on the applied heat flux, but were unexpectedly independent of vapor quality, which is contrary to large diameter channel trends. Similar results were obtained by Tran et al. (1996) and Bao et al. (2000). Tran et al. performed experiments on R-12 in circular and rectangular channels with sizes ranging from 2.40 to 2.92 mm. Their data showed that for a sufficiently high wall superheat (above 2.75 K), the values of the heat transfer coefficient were unaffected by vapor quality and mass velocity, but increased significantly with heat flux. The flow boiling experiments of Bao et al. again confirmed these trends and presented additional data showing the improvement in heat transfer with increasing saturation pressure, further promoting the view that nucleate boiling was dominating the process (no visualization of the flow was possible in their setup). More recently, Lihong et al. (2005) performed experiments on a 1.3-mm circular channel for refrigerant R-134a, yielding similar results.

Added trends in heat transfer were reported by Lin et al. (2001). In their study on R-141b (1.1 mm tube), they observed three distinct trends in the heat transfer coefficient to changes in heat flux and vapor quality: (1) at low

heat fluxes, heat transfer improved with increasing vapor quality, (2) for intermediate values and vapor qualities within 0.40, heat transfer increased with heat flux, much like what was observed in the investigations cited previously, and (3) at the highest heat fluxes, heat transfer gradually fell with vapor quality and tended to heat flux independent values. While further heating increased the heat transfer coefficient for vapor qualities up to 0.40, this effect was much less evident beyond this threshold.

Saitoh et al. (2005) obtained heat transfer data for boiling of R-134a in a 0.51 mm tube (550 mm long) at 15 and 29 kW/m^2 for vapor qualities extending to almost unity. Their heat transfer coefficients showed an inverted "U" shape in the α-x plane. The heat transfer data increased up to a vapor quality of 0.60, beyond which the coefficients declined monotonically. In another study on R-134a, Martín-Callizo et al. (2007) presented results for a vertical 0.64 mm stainless steel micro-channel, finding that once again the dominant effect was that of heat flux while mass velocity was less important. They found that their heat transfer coefficients were rather insensitive to vapor quality until reaching the higher end of their heat flux test range, where upon the heat transfer coefficients then decreased monotonically from vapor qualities of about 0.01–0.02 down to values of about 0.6–0.8 without going through any maximum or minimum.

As for the effect of mass velocity, a number of investigations have shown that heat transfer coefficients remain unchanged when varying the fluid flow rate (which is counter-intuitive with respect to boiling in macro-channels), as in the data from Tran et al. (1996). Tran et al. reported an improvement in heat transfer with mass velocity only for wall superheats lower than 2.75 K. The experiments of Bao et al. (2000) on R-11 and R-123 and Lihong et al. (2005) on R-134a, also showed no change in heat transfer with flow rate, with the latter observing mild differences only at the lowest heat flux tested. One of the few studies on a single channel that presented a different outcome was that of Sumith et al. (2003) for flow boiling of water in a 1.45 mm vertical tube, reporting heat transfer coefficients that often decreased when increasing the flow, even at high heat fluxes.

At present, there is general agreement that a higher saturation pressure/temperature yields higher heat transfer coefficients when boiling in micro-channels [see for example Bao et al. (2000), Lihong et al. (2005), Shiferaw et al. (2007), and Martín-Callizo et al. (2007)]. Similar results have also been recently reported in flow boiling heat transfer experiments on multi-micro-channel systems, as in the case of Agostini et al. (2008a, b) who tested refrigerants R-134a and R-236fa in a 67 parallel micro-channel evaporator (rectangular channels, 0.223 mm wide, 0.680 mm high and 20.0 mm long, separated by 0.80 mm wide fins).

Their heat transfer data at low heat fluxes tended to increase with vapor quality until intermediate heat fluxes, where they first increased and then showed nearly no influence of vapor quality. At higher heat fluxes, the heat transfer coefficients started to decline with increasing vapor quality. While the heat transfer coefficients increased sharply with increasing heat flux, at the highest values (starting at 178.4 W/cm^2 relative to the base surface area of the heating element), a peak was reached and the heat transfer coefficients began to decrease with heat flux as the critical heat flux was approached (but not reached).

The present study aims to provide further insight into two-phase single micro-channel heat transfer, through a sensitivity analysis on the effect of the different operational parameters, fluid properties, and channel size on thermal performance. The current database includes results for three different refrigerants, R-134a, R-236fa and R-245fa, two channel diameters, 510 and 790 μm, mass velocities from 300 to 2,000 kg/m^2 s, and heat fluxes up to 200 kW/m^2.

2 The experimental set-up

The experimental test stand is illustrated in Fig. 1 and includes two pressurized vessels, a Coriolis mass flowmeter (CMF), a flow adjustment valve, and the test section. All tubing, other than for the test section, is 4 mm in internal diameter. The flow is driven by the pressure difference between the two temperature controlled vessels, each of which contains saturated liquid and vapor. The vessels are thus maintained at different pressures/temperatures by means of external thermal regulating units. This setup avoids having to use components with moving parts, i.e. a pump, which may induce undesirable vibrations to the fluid and
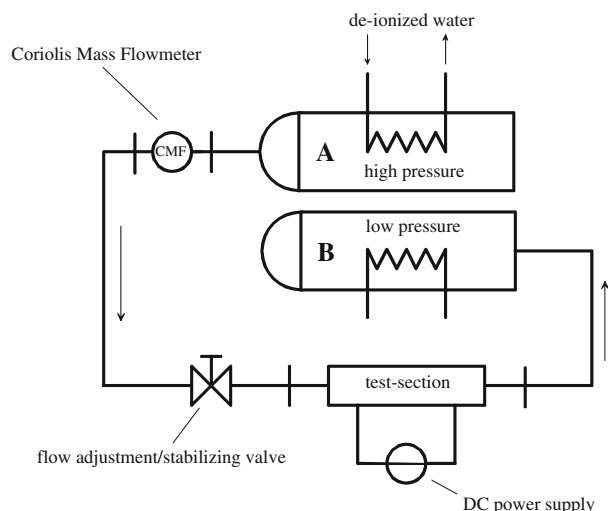
Fig. 1 A schematic diagram of the experimental facility

allows operation over a very wide range of flow rates. Saturated liquid, extracted from the bottom of the high pressure tank, crosses the CMF, enters the test section through the valve, and is then directed into the low pressure vessel.

The fluid at the inlet to the valve must be sub-cooled to avoid flashing. For this reason, the first tank (vessel A in Fig. 1) is always kept above ambient temperature. Heat is lost by the flow to the surroundings as it approaches the valve, where the liquid is at approximately ambient temperature, and an adequate degree of sub-cooling is generally guaranteed. If, however, flashing should occur, the two-phase flow would be detected through a sight glass positioned immediately after the valve.

The operating conditions are set by acting on the temperature of the refrigerant within the two vessels, by adjusting the opening of the valve, and by regulating the current to the pre-heater and evaporator in the test section. The valve also has a stabilizing effect on the flow, avoiding the onset of (1) excursive (Ledinegg) instabilities, which may lead to critical conditions in the test section, and (2) oscillatory instabilities, by inhibiting back-flow of liquid.

Before starting any experimental run, vessel A is charged with refrigerant from vessel B, by an oil-free external pump. Once the filling procedure is completed, the connection with vessel B is closed, the pump is stopped and disconnected, and the two reservoirs are left to equilibrate at their respective temperatures.

The test section, illustrated in Fig. 2, includes the micro-channel, all the connections to the electric power supply units, and the instrumentation required for the measurements. The three main sectors of the test section are (1) the pre-heater, for setting the desired inlet conditions to the evaporator, (2) the evaporator, where boiling occurs and heat transfer is measured, and (3) the glass tube for flow visualization. All three channels have the same internal diameters, and the junctions between each sector are manufactured to allow for precise alignment. Both the pre-heater and evaporator are made from stainless steel, and each has a pair of copper electrodes to electrically heat the channel and thus the flow (by a DC current). Two pressure taps are located immediately upstream and downstream of the test section, while type K thermocouples (50 μm leads) are positioned on the outer walls of both the pre-heater and evaporator. The thermocouple leads are placed within individual support shells to avoid breakage, and their hot junctions are pressed against the tube wall through external

Fig. 2 a A schematic diagram of the flow boiling test section showing the two pressure taps (p) at the inlet and exit, and the location of the pre-heater (PH) and evaporator (EV) thermocouples, and b an image of the evaporator within the test section
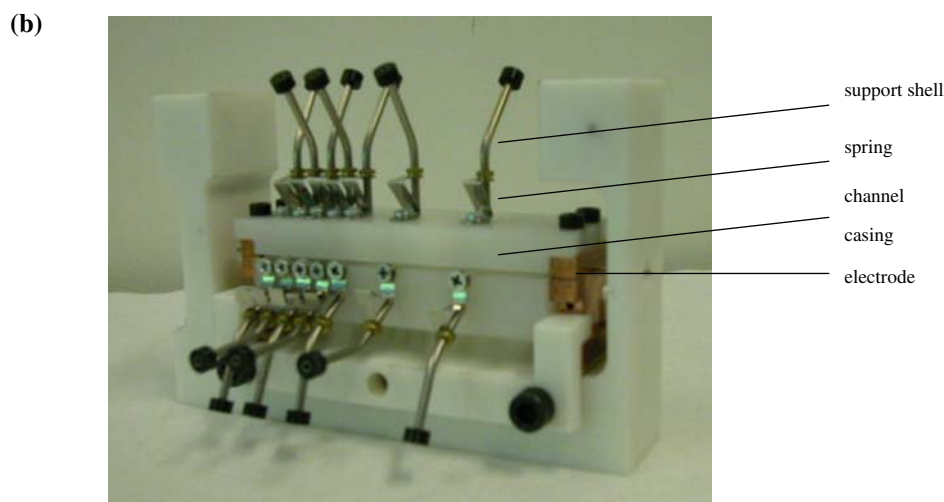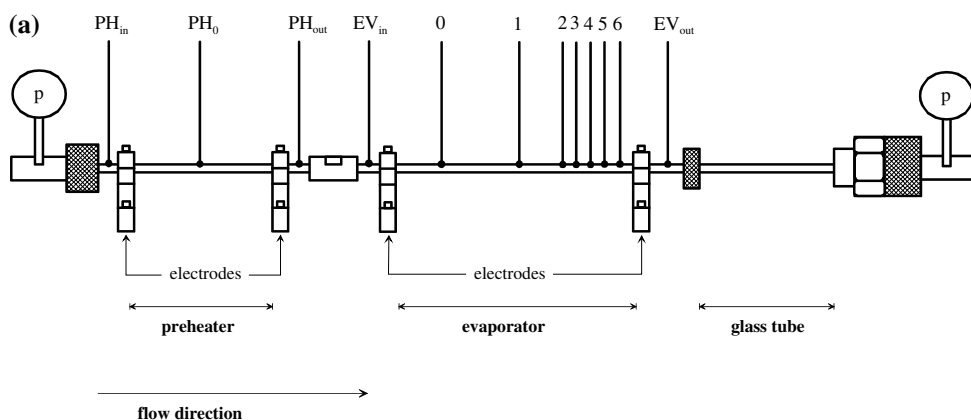
springs thus reducing contact resistance (see Fig. 2b). A fine layer of insulating varnish is placed between the junction and the tube wall to avoid electrical disturbance of the thermocouple measurement.

Inlet and outlet fluid temperatures are obtained from wall temperature measurements taken at the two adiabatic locations before and after the heated lengths (see Fig. 2a). Numerical heat conduction simulations showed that their values were not affected by axial conduction. The other thermocouples, positioned between the electrodes, provide the outer temperatures of the wall that are then used to determine the local heat transfer coefficients. The two pairs of electrodes (pre-heater and evaporator) are connected to two separate DC power supplies. The intensity of the applied current is measured by a current intensity meter, while the voltage drop is measured directly at the electrodes. Table 1 provides the technical specifications of the test section.

The two measured inner diameters of the evaporator for the current study are of 510 and 790 μm (Table 1). Their interior roughnesses were measured by laser profilometry, giving mean absolute values of 2.41 ± 0.12 μm for the 510 μm channel and 1.75 ± 0.27 μm for the larger channel.

3 Test fluids

The test fluids are three single-component refrigerants: R-134a, R-236fa, and R-245fa. Figure 3 compares schematically their physical properties at a saturation temperature of 31°C, which corresponds to the value for most of the present experimental runs. The three main properties that distinguish each refrigerant are surface tension, vapor density, and liquid viscosity. The surface tension of R-245fa exceeds the value of R-134a by over 80%. R-245fa also presents a vapor density that is lower than that of R-134a by 60%, while being much more viscous (over +100%). R-236fa positions itself at an intermediate level with respect to the other two fluids. While the combined effect of a low vapor density and a high liquid viscosity

will enhance pressure drop, a reduction in ρ_v will increase the degree of expansion associated with phase change. As for surface tension, the bubble departure diameter (d_d), taken to be proportional to the capillary length scale, i.e. $d_d \propto [\sigma/(\rho_l g)]^{1/2}$ for $\rho_v \ll \rho_l$, is expected to increase with σ, and may lead to a reduction in departure frequency for the high surface tension fluid.

4 Data reduction

Local heat transfer coefficients are evaluated at every temperature measurement point on the heated length of the evaporator. The heat transfer coefficient, α, is defined in terms of the magnitude of the wall heat flux (q), and the difference between the inner wall temperature (T_w) and that of the bulk fluid (T_f):
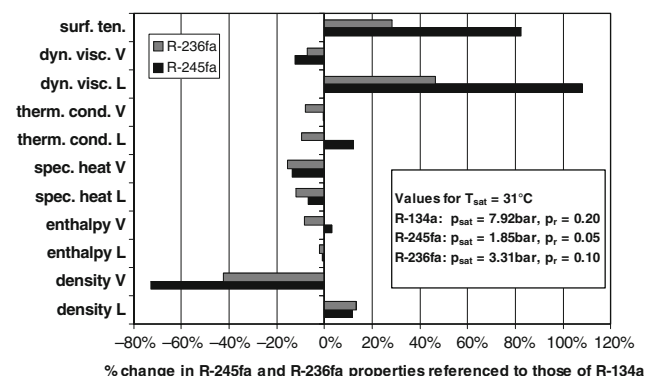
$$\alpha \equiv \frac{q}{T_w - T_f} \tag{1}$$

The temperature of the inner wall is derived by correcting the measured values at the outer wall assuming one-dimensional radial conduction with internal generation of heat (q_g'''),

$$T_w = T_1 + \frac{q_g''' D_1^2}{k_w} \left[1 - \left(\frac{D}{D_1}\right)^2 + 2\ln\left(\frac{D}{D_1}\right) \right] \tag{2}$$

with k_w the thermal conductivity of the wall, T_1 the temperature at the outer surface, and D_1 and D respectively the outer and inner diameters of the tube. Equation 2 is thus used to correct the temperature readings of the thermocouples. The internal heat generation term in Eq. 2 is evaluated from the voltage drop at the electrodes of the evaporator (V), and the current intensity (I):

$$q_g''' = \frac{4\eta\, IV}{\pi\left(D_1^2 - D^2\right) L} \tag{3}$$

Table 1 Size and material characteristics of the test section

Tube material	AISI 304
Inner tube diameters (μm)	510, 790
Outer tube diameters (μm)	690, 1,000
Pre-heater heated length (mm)	43
Evaporator heated length (mm)	75
Glass tube inner diameter (μm)	520, 800
Glass tube length (mm)	100

Fig. 3 Graphic comparison of the physical properties of the three refrigerants tested at 31°C

with η the thermal efficiency of the system, which accounts for heat losses from the test section, and L the tube length. The wall heat flux, q_w, is then given as

$$q_w = -k_w \frac{dT}{dr}\bigg|_{r=D/2} = -\frac{q_g'''}{4D}(D_1^2 - D^2) = -\frac{\eta IV}{\pi DL} \quad \text{and}$$

$$q = |q_w| = \frac{\eta IV}{\pi DL} \tag{4}$$

Although the thermal resistance of the flow is relatively low, part of the supplied heat is dissipated elsewhere. There are five main sources of heat losses from the channel: (1) heat losses by natural convection to the surrounding ambient, (2) heat removed by axial conduction at the channel entrance and exit, (3) heat conducted through the thermocouple lead wires, (4) radiation heat losses to the ambient, and (5) heat losses by conduction through the electrodes and power cables. The last three sources for heat losses were found to be negligible for the present experimental conditions, since the operating temperatures are fairly close to the ambient temperature ($T_1 \leq 48°C$) and the cross-sectional area of the thermocouple leads is very small (2×10^{-3} mm^2). The overall heat loss, $\dot{Q}_{loss}$, from the evaporator may be therefore expressed as

$$\dot{Q}_{loss} \cong \dot{Q}_{cond} + \dot{Q}_{conv} \tag{5}$$

where the first term on the right-hand side of Eq. 5 refers to the losses by longitudinal conduction at the extremities of the evaporator, while the second refers to those due to natural convection. Defining the heating efficiency, η, as

$$\eta = \frac{\dot{Q}}{IV} = 1 - \frac{\dot{Q}_{loss}}{IV} \tag{6}$$

where $\dot{Q}$ is the thermal power delivered to the flow, while IV is the heating rate by Joule effect, Eq. 6 may be rewritten as

$$\eta = 1 - \varepsilon_{cond} - \varepsilon_{conv} \quad \text{with} \quad \varepsilon_{cond} = \frac{\dot{Q}_{cond}}{IV} \quad \text{and}$$
$$\varepsilon_{conv} = \frac{\dot{Q}_{conv}}{IV} \tag{7}$$

The conduction losses are obtained by a one-dimensional axial conduction calculation, giving the following form to ε_{cond},

$$\varepsilon_{cond} = 2\frac{\cosh(\sqrt{Bi}) - 1}{\sqrt{Bi}\,\sinh(\sqrt{Bi})} \quad \text{with} \quad Bi = \frac{\alpha}{k_w}\left(\frac{4L^2 D}{D_1^2 - D^2}\right) \tag{8}$$

the tube Biot number. On the other hand, the relative losses by natural convection to the ambient are assessed utilizing the Churchill and Chu (1975) correlation developed for isothermal horizontal cylinders,

$$Nu_\infty = \left\{0.60 + \frac{0.387 Ra^{1/6}}{\left[1 + \left(\frac{0.559}{Pr_\infty}\right)^{9/16}\right]^{8/27}}\right\}^2 \tag{9}$$

where the average outer wall temperature is used in the computation of the Rayleigh number.

In most experiments, the fluid at the exit of the pre-heater is sub-cooled. Thus, the evaporator begins with a sub-cooled region followed by one in which the flow is saturated. Although zones with sub-cooled boiling or superheated liquid may also occur, the following procedure neglects their presence, assuming the flow to exhibit thermodynamic stability and equilibrium. The sub-cooled length, z_{sat} (having taken $z = 0$ at the entrance to the evaporator), and the local saturation pressure and temperature ($p = p_{sat}$ and $T = T_{sat}$ at $z = z_{sat}$) are given by the following set of equations:

$$q\,\pi D\,z_{sat} = \frac{1}{4}G\,\pi D^2 \int_{T_{in}}^{T_{sat}} c_p(p,T)\,dT \tag{10}$$

$$p_{sat} = p_{in} - 4f\left(\frac{z_{sat}}{D}\right)\frac{G^2}{2\rho_l} \tag{11}$$

$$T_{sat} = T_{sat}(p_{sat}) \tag{12}$$

Equation (10) is an energy balance over the sub-cooled length, with c_p the specific heat of the liquid expressed by a third degree polynomial of the local temperature (the effect of pressure is neglected). Equation 11 gives the pressure drop experienced by the sub-cooled liquid flow, where f is Fanning's friction factor, computed as $16/Re$ for laminar flow, or, in the case of turbulent flow, as $0.079/Re^{0.25}$ (Blasius' expression for smooth tubes). The third equation, Eq. 12, yields the saturation temperature as a function of pressure, and, as in the case of c_p, a third degree polynomial accurately represents the dependency in the range of conditions tested. The values of the three unknowns, namely, z_{sat}, T_{sat}, and p_{sat}, are given by the simultaneous solution of the above set equations.

The evaporation of the flow is assumed to start at $z = z_{sat}$, where the local vapor quality is zero. Beyond z_{sat}, the saturated two-phase flow experiences an increase in vapor quality primarily due to heating, although frictional and momentum pressure losses also contribute. The vapor quality, defined as the ratio of the flow rate of the vapor phase to the total mass flow rate, may be expressed in terms of local enthalpies, i.e.

$$x = \frac{h - h_l}{h_{lv}} \tag{13}$$

where h_l and h_{lv} are respectively the liquid specific enthalpy and the latent heat of vaporization computed at

the local pressure. Equation 13 extends the concept of vapor quality to sub-cooled liquid flows, in which case it will assume negative values. The enthalpy of the fluid, h, at a location z along the channel is given by the energy balance

$$h(z) = \frac{4\,q}{GD} z + h_0 \tag{14}$$

with h_0 the specific enthalpy of the flow at the entrance to the evaporator (at $z = 0$). Equation 14 neglects the change in kinetic energy of the vaporizing flow, since it is generally small compared to the other contributions.

To assess the fluid properties in Eq. 13, and to estimate the local temperature of the two-phase flow, an expression for the pressure gradient in the saturated length must be assumed. At present, however, no reliable pressure drop models or correlations are available for micro-channel two-phase flows. In this study, the two-phase pressure gradient is assumed to be constant and the local pressure is thus

$$p(z) = p_L + \frac{p_{sat} - p_L}{z_{sat} - L}(z - L) \tag{15}$$

Here p_{sat} is the pressure at $z = z_{sat}$, as calculated from Eq. 11, and p_L is the outlet pressure (relative to $z = L$). The pressure p_L is known from the measured value of the outlet temperature, and Eq. 15 may thus be used to compute the local fluid temperature through the same polynomial as in Eq. 12.

5 Measurement uncertainties

The error on any directly measured physical quantity is determined utilizing the indication of the probe manufacturer and through analysis based on in-house calibration and data regression of all instrumentation. The thermocouples were calibrated with an uncertainty of $\pm 0.15°C$, while the error on the pressure at the evaporator inlet was computed to be ± 12 mbar. The uncertainty on the local vapor quality was estimated by error propagation analysis

to be as high as 50% of the value for very low vapor qualities (i.e. $x < 0.05$), while for $x > 0.05$ the uncertainties reduced to $<10\%$ of the value. The inner diameter of the channel was measured using measurement needles of increasing sizes, with the following mean values and corresponding uncertainties: (i) $D = 510 \pm 10$ μm, and (ii) $D = 790 \pm 10$ μm. Table 2 illustrates the upper and lower limits to the uncertainties for a selection of the main experimental parameters.

6 Validation by single-phase tests

Research on single-phase micro-channel flows has addressed the issue as to whether very small channels induce a difference in heat transfer and pressure drop with respect to conventional theory for macro-scale systems. Although at present the issue is not entirely resolved, several recent investigations (see Celata 2005) have provided evidence to support the conclusion that the underlying mechanisms remain unaltered. From this perspective, numerous single-phase heat transfer experiments have been performed in the present study to validate the test setup prior to the two-phase measurements. Figure 4a presents results for sub-cooled liquid flows of R-134a. Generally, the data in the transition-turbulent region give satisfactory agreement with well-established single-phase correlations. When compared to the Gnielinski and Dittus–Boelter correlations, the average experimental Nusselt numbers position themselves in between the two predictions and the slight discrepancy may be attributed to the uncertainty in the measurements.

Single-phase flow experimentation also allows for an indirect measurement of η, Eq. 7, since assessing the effective heat input to the flow simply requires the flow rate, the specific heat of the fluid, and the inlet and exit fluid temperatures. Figure 4b illustrates one set of heat balance results for an experiment on a sub-cooled liquid flow of R-134a. The plot, which shows η as a function of the electrical heat input (IV), presents an average thermal

Table 2 Uncertainties on mass velocity, heat flux, and heat transfer coefficient for the tested fluids

	R-134a				R-236fa				R-245fa			
	510 μm		790 μm		510 μm		790 μm		510 μm		790 μm	
	Min (%)	Max (%)	Min (%)	Max (%)	Min (%)	Max (%)	Min (%)	Max (%)	Min (%)	Max (%)	Min (%)	Max (%)
Mass velocity	4		3		4		3		4		3	
Heat flux	3	11	2	5	3	4	2	8	4	10	2	5
Heat transfer coefficient	6	22	4	24	5	20	4	27	5	20	3	25
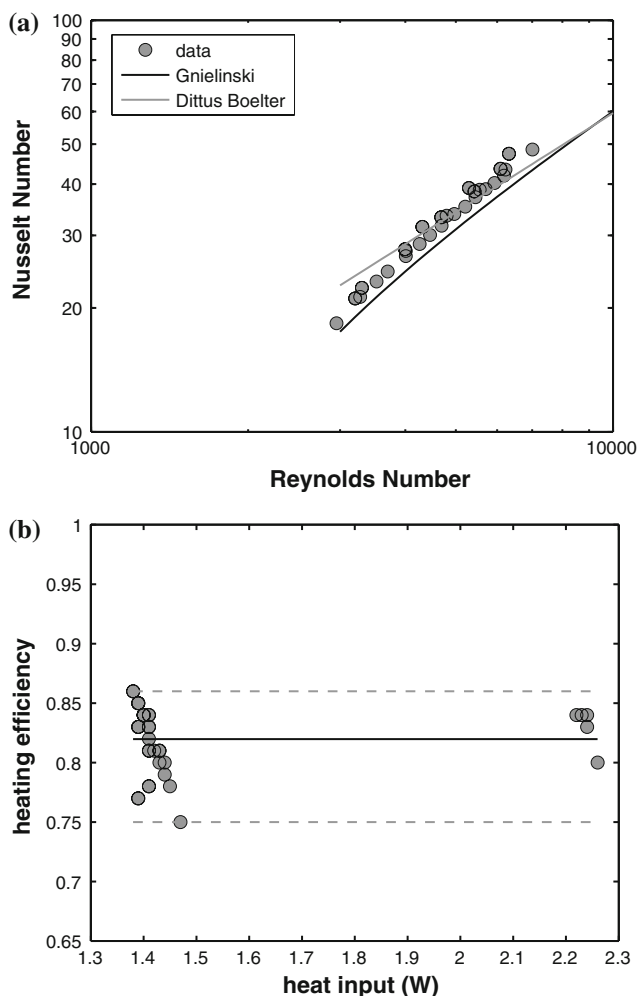
Fig. 4 a Single-phase Nusselt numbers and **b** heat balance for sub-cooled liquid flows of R-134a in the 510 μm micro-channel

efficiency of 82%. When performing single-phase tests on heat dissipation, the level of heat flux is small to maintain the wall below the corresponding fluid saturation temperature, thus avoiding the onset of sub-cooled boiling. The measured thermal efficiencies are then compared to the predictions by Eq. 7, to validate the computation that is then applied to the reduction of the flow boiling data. During flow boiling experiments, the computed heat loss from the test section to the environment is usually less than 10%.

7 Flow boiling heat transfer results

In the current section, stable flow boiling heat transfer coefficients are presented, while in the next section the unstable flow boiling heat transfer data are described. The distinguishing factor between experiments which are

deemed to be stable from those which are affected by instability is the degree of fluctuation in the measured parameters. The following stable flow data present quasi-steady outer wall temperatures, whose fluctuations are within the uncertainty band of the individual thermocouples.

7.1 Flow boiling curves

Figure 5 illustrates two typical flow boiling curves for R-134a and R-245fa in the 510 μm channel. The data refer to the last temperature measurement location, 65 mm downstream from the entrance to the evaporator, and are obtained by varying the intensity of the supplied current, or, in other terms, the heat flux. In both cases the wall superheat, defined as the difference between the inner wall temperature and the saturation temperature at the local pressure, is shown to experience a substantial excursion before reaching the boiling onset when increasing the heat flux, with values as high as 30–35°C for R-245fa and R-236fa (the latter not shown). The boiling branches of the curves present no hysteresis, with the data for ascending and descending heat fluxes substantially in agreement with one another. While not shown here, the repeatability of the boiling tests was very good.

Some visualizations taken at the exit to the evaporator, assumed to be consistent with the flow patterns occurring at the last measurement site, are illustrated to the left of each boiling curve. While R-134a presents the four typical flow patterns (bubbly, slug, churn, and annular flows), the bubbly and slug flow patterns for R-245fa are less evident since at even very low heat fluxes the flow is seen to have churn flow characteristics.

7.2 Two-phase heat transfer for R-134a

Figure 6 depicts R-134a flow boiling heat transfer coefficients for four different mass velocities at heat fluxes ranging from 12 to 200 kW/m^2. The applied heat flux is limited by the critical heat flux (which was avoided here). The data, plotted on the α-x plane, show heat transfer coefficients that change relatively little with vapor quality and that increase with heat flux. The value of α is as high as 35 kW/(m^2 K) at a heat flux of 200 kW/m^2. The effect of mass velocity is better seen in Fig. 7, where the heat transfer coefficients are plotted for two heat fluxes and mass velocities between 250 and 800 kg/(m^2 s). Other than for a certain degree of experimental scatter, the data points at a fixed heat flux overlap, indicating a minimal effect of mass velocity.

Figure 8 illustrates the effect of inlet sub-cooling and saturation temperature on the two-phase heat transfer coefficients. The saturated flow boiling coefficients are unaltered by changes in the temperature of the sub-cooled

Fig. 5 Flow boiling curves and flow patterns for (**a**) R-134a and (**b**) R-245fa in the 510 μm micro-channel, relative to the last temperature acquisition location on the heated length
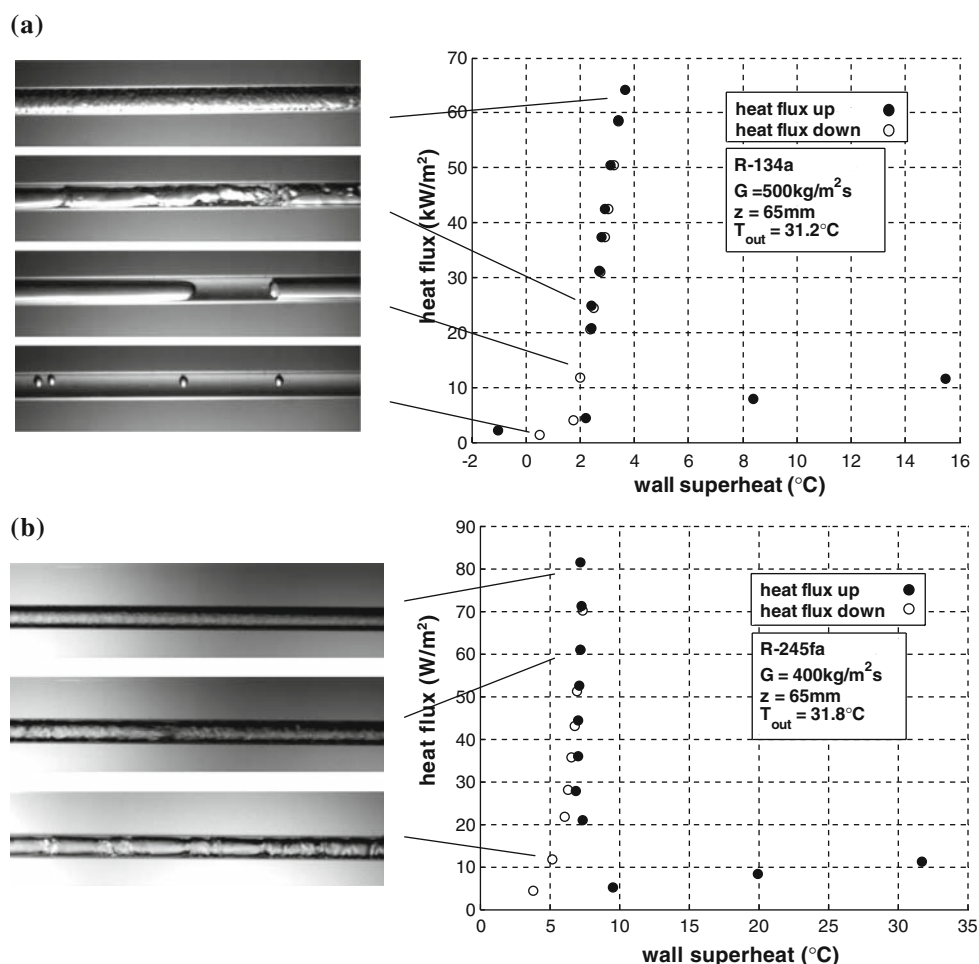
liquid entering the evaporator (Fig. 8a), while the values of α generally benefit from higher saturation temperatures/pressures over a wide range of heat fluxes (see Fig. 8b, where mean values for the saturated zone of the test section are plotted to simplify the illustration of this point).

The observations above for the 510 μm tube are generally reconfirmed when testing the larger size channel ($D = 790$ μm). Figure 9 illustrates heat transfer coefficients for a high mass velocity test. When comparing the average heat transfer coefficients to help highlight the relative performances, reducing the tube size is seen to enhance heat transfer (as in Fig. 9b).

Shiferaw et al. (2007) performed experiments with R-134a in 2.01 and 4.26 mm circular stainless steel channels, under similar conditions to some of the data sets presented above. Figure 10 illustrates the direct comparison between the current study and Shiferaw et al. (2007) for a mass velocity of 300 kg/m² s. Shiferaw's data for the 2.01 mm tube agree quite well with the present values for the 510 μm channel at corresponding levels of heat flux, and any discrepancy may be associated with the difference in tube size. The tube diameter effect seems to be more manifest at the lower heat fluxes, disappearing at the higher

values. A similar conclusion may be drawn from the comparison of data from Shiferaw's 4.26 mm channel with current data for the 790 μm tube, although in this case the effect of channel diameter is less clear.

7.3 Two-phase heat transfer for R-236fa

The results for R-236fa present many similarities to those for R-134a. As shown in Fig. 11, the heat transfer coefficients are extremely sensitive to heat flux, and reveal a limited influence of mass velocity and vapor quality. As for R-134a, the data for R-236fa showed an improvement in heat transfer with saturation temperature, while no substantial change was observed when varying the degree of inlet sub-cooling. Tests for the larger channel yield similar trends in the α-x plane, and the average values of the heat transfer coefficients were again lower than those in the 510 μm channel. Here, however, the effect of tube diameter increased with heat flux (Fig. 12).

Under the present test conditions, R-236fa distinguishes itself from R-134a mainly in the magnitude of the heat transfer coefficients. The values of α for R-134a are generally about twice those of R-236fa.
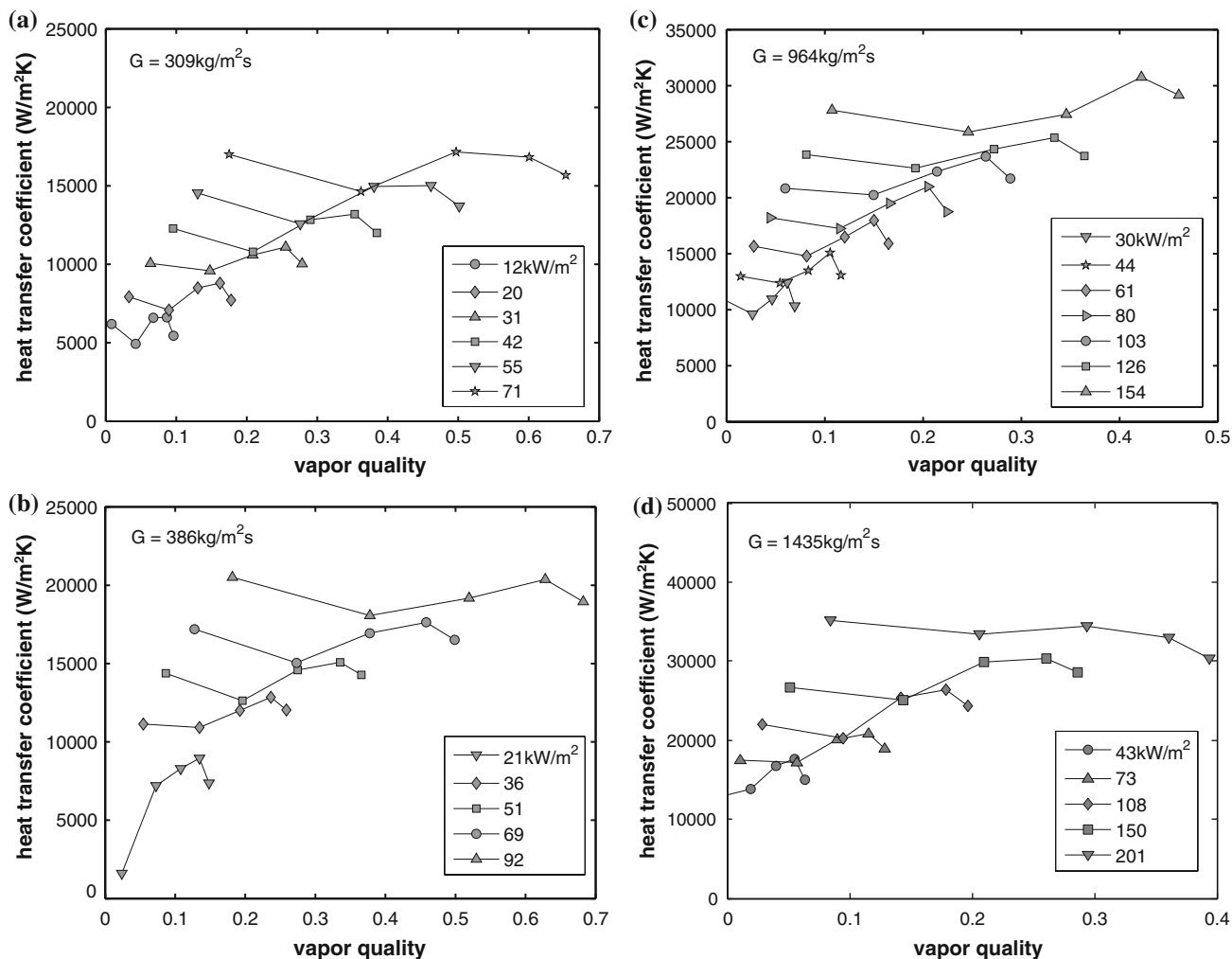
Fig. 6 Experimental heat transfer coefficients versus vapor quality for saturated flow boiling of R-134a in the 510 μm micro-channel for (**a**) 309, (**b**) 386, (**c**) 964, and (**d**) 1,435 kg/m² s. The flow enters the channel as a sub-cooled liquid at 29°C, and exits as a saturated two-phase fluid at 31°C
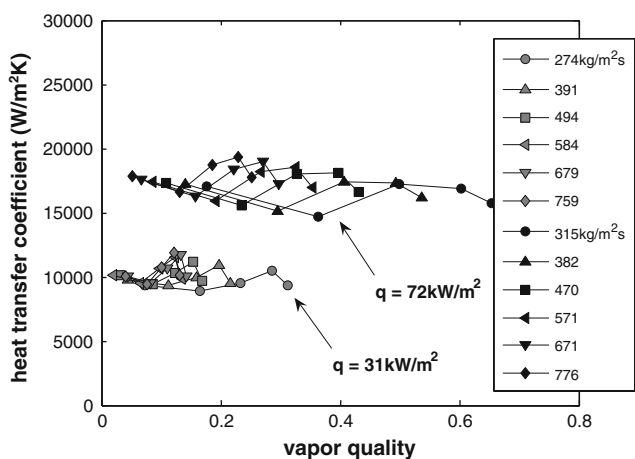
Fig. 7 Experimental heat transfer coefficients for R-134a in the 510 μm micro-channel, over a range of mass velocities at two heat fluxes. The flow enters the channel as a sub-cooled liquid at 29°C, and exits as a saturated two-phase fluid at 31°C

7.4 Two-phase heat transfer for R-245fa

The trends in the data for R-245fa present some distinctively different characteristics with respect to those seen for the previous two fluids. Figure 13 shows a plot for a representative set of heat transfer coefficients in the α-x plane. Unlike the results for R-134a and R-236fa, heat transfer for R-245fa appears to be sensitive to heat flux only up to intermediate vapor qualities, beyond which the data points for different values of q merge, and exhibit a monotonic increase with vapor quality. The heat transfer coefficients corresponding to the highest heat flux (110 kW/m²) in Fig. 13 are affected by irregular spikes in the wall temperatures, indicating the approach to the critical heat flux condition. Figure 14 illustrates two other sets of heat transfer data for mass velocities of 300 and 800 kg/m² s. Figure 14a shows similar results to the ones in Fig. 13, with the only difference in the trend of data for
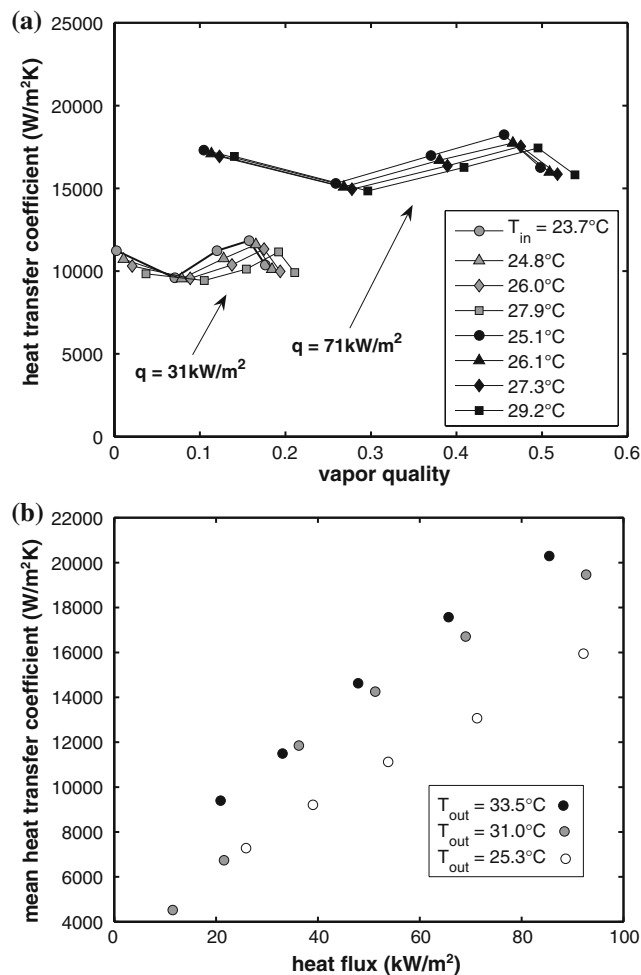
Fig. 8 a Experimental heat transfer coefficients for R-134a at 31°C and different inlet temperatures, and **b** average heat transfer coefficients versus heat flux for three different outlet fluid temperatures. The results refer to the 510 μm micro-channel at a nominal mass velocity of 400 kg/m² s
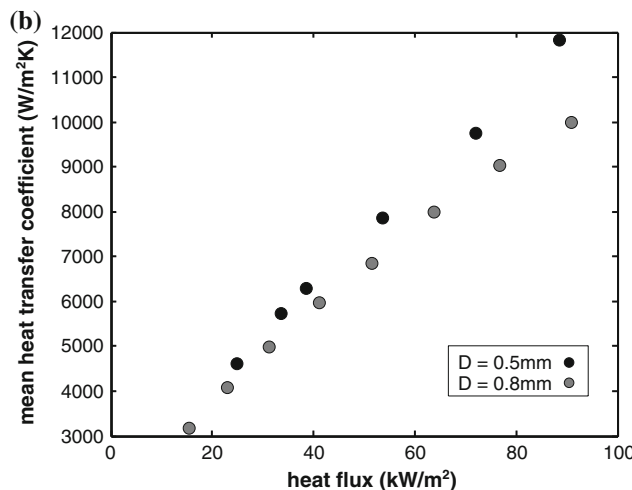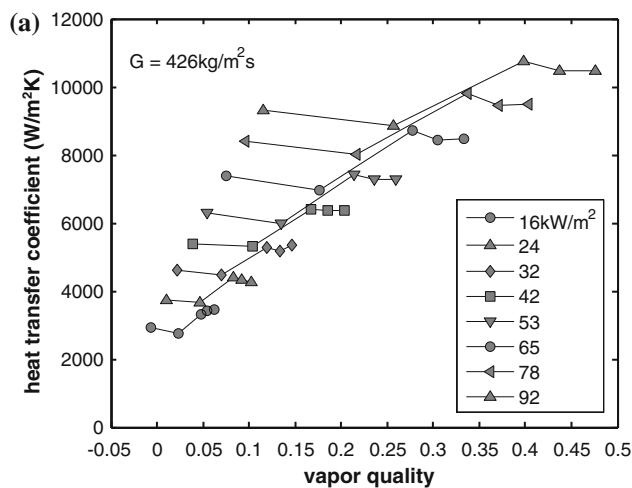
Fig. 9 a Experimental heat transfer coefficients versus vapor quality in the 790 μm channel, and **b** average heat transfer coefficients versus heat flux for the two tube sizes. The data refer to flow boiling of R-134a with an outlet temperature of 31°C and a nominal mass velocity of 1,000 kg/m² s

$q = 53$ kW/m², which was subjected to an oscillatory instability. The heat transfer coefficients in Fig. 14b cover a more limited range of vapor qualities, and show the dependency on heat flux at the medium-low values of x. As for R-134a and R-236fa, these heat transfer characteristics are also found for the larger tube, although in this case the coefficients drop with vapor quality in the heat flux dependent region (low x), and, as for the smaller channel, merge as vaporization progresses.

8 Comparison of heat transfer predictions to the experimental data

Figures 15 and 16 present the overall comparison of a selection of methods developed for micro-channel flow boiling with the current database. Figure 15 refers to the methods of Lazarek and Black (1982), Tran et al. (1996), Kandlikar and Balasubramanian (2004), and Zhang et al.
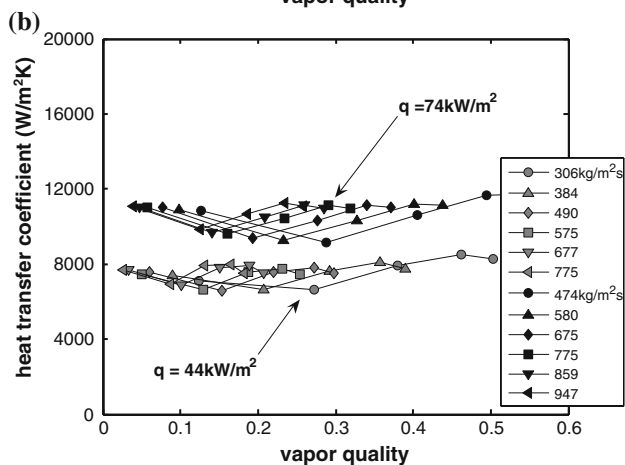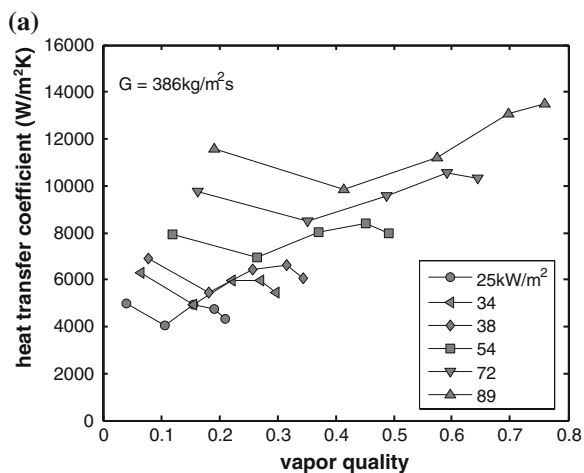
(2004). Lazarek and Black's correlation gives the highest success rate, with 88% of the data predicted within ±30% (relative to the experimental values), while the one by Tran et al. performs the worst, with only 4% within the same error band. Although the correlation by Zhang et al. predicts only 58% of the data in the ±30% range with a general tendency to under-predict the experimental coefficients, it is also the method with the lowest degree of dispersion. Figure 16 refers to the three-zone evaporation model of Thome et al. (2004). The first figure (Fig. 16a) is a comparison of the model with the entire database, while the second (Fig. 16b) considers only those data points for which the corresponding flow is in either isolated bubble (ib) mode or coalescing bubble (cb) mode (given by the flow pattern map of Revellin and Thome 2006), as the three-zone model is for the elongated bubble (slug) flow regime. As shown in Fig. 16, the 59% success rate increases to 77% when the data is segregated according to flow pattern.
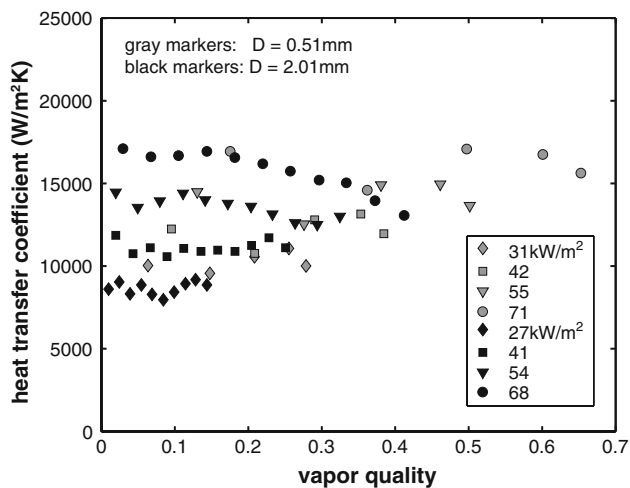
Fig. 10 Comparison with present data to those of Shiferaw et al. (2007) for R-134a. *Black markers* refer to the data from Shiferaw ($G = 300$ kg/m² s and 8 bar), while *white markers* refer to the current database ($G = 309$ kg/m² s and $p_L = 7.92$ bar)
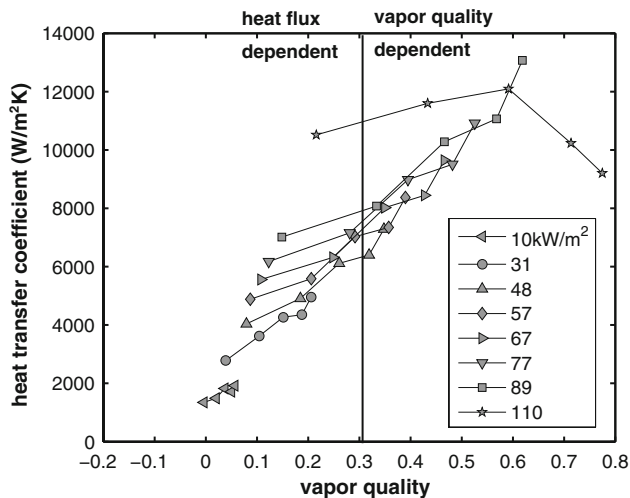

Fig. 11 Experimental heat transfer coefficients for flow boiling of R-236fa in the 510 μm channel for (**a**) $G = 386$ kg/m² s and different heat fluxes, and (**b**) different mass velocities. In both cases, $T_0 = 29°C$ (*inlet*) and $T_L = 31°C$ (*exit*)

Fig. 12 **a** Experimental heat transfer coefficients of R-236fa versus vapor quality in the 790 μm channel, and **b** average heat transfer coefficients versus heat flux for the two tube sizes. The data refer to flow boiling with $T_L = 31°C$ and a nominal mass velocity of 400 kg/m² s

Sets of data were examined versus the corresponding predictions of the methods. Lazarek and Black's correlation predicted the order of magnitude of the heat transfer data with some success, and is consistent with the trend in the data for R-134a and R-236fa that show little change with vapor quality. Clearly, problems started occurring once the data showed a dependency on vapor quality, as in the case of R-245fa, and the general applicability of the correlation becomes questionable. For R-245fa the heat flux independent behavior described in the previous section develops primarily in the annular flow region, and is not captured by any of the methods.

## 9 Flow boiling with oscillatory instabilities

The heat transfer data presented thus far refer to stable micro-channel two-phase flows; i.e. flows that present no

Fig. 13 Experimental heat transfer coefficients for R-245fa plotted versus vapor quality for flow boiling (510 μm channel) at a mass velocity of 400 kg/m^2 s, with an inlet temperature of 30°C and exiting at 32°C

substantial oscillation in the measured parameters and that are thus characterized by an unambiguous steady-state. Figure 17a illustrates a representative "stable" temporal profile for the outer wall temperature, with the fluctuations generally within the uncertainty band of the thermocouples. Flow stability is guaranteed by the presence of the valve at the entrance to the test section (see Fig. 1), which "isolates" the boiling flow in the evaporator from any upstream compressibility (Bergles and Kandlikar 2005). As the valve is opened, while maintaining fixed operating conditions by adjusting the pressures in the two vessels, the resistance to backflow is reduced. If the conditions are such that the pressure pulse from the bubble formation process is strong enough, an oscillatory instability will propagate, with liquid being cyclically expelled in both directions. In Fig. 17b for an unstable flow, the temperature fluctuation with respect to the mean is about ±2.0°C, much higher than ±0.15°C of the equivalent stable flow. Furthermore, the temperature cycle is quite repeatable in both shape and magnitude, with a frequency of about 4 Hz. Other studies mentioning unstable flows (see Kenning and Yan 2001, and Brutin et al. 2003) have also noted frequencies of this magnitude.

Once the flow becomes unstable, the outer wall temperature profiles change dramatically, as shown in Fig. 17b. The temperatures start oscillating very regularly, with amplitudes that increase with heat flux. Figure 18 illustrates the progressive rise in the intensity of the oscillation with heat flux, for an unstable flow of R-236fa. Higher heating also changes the shape of the curves. Figure 19 shows a set of results for R-245fa. The low heat flux case presents two main oscillation modes in the temperature of the heated wall at 4.4 and 7.3 Hz. As the heat flux is
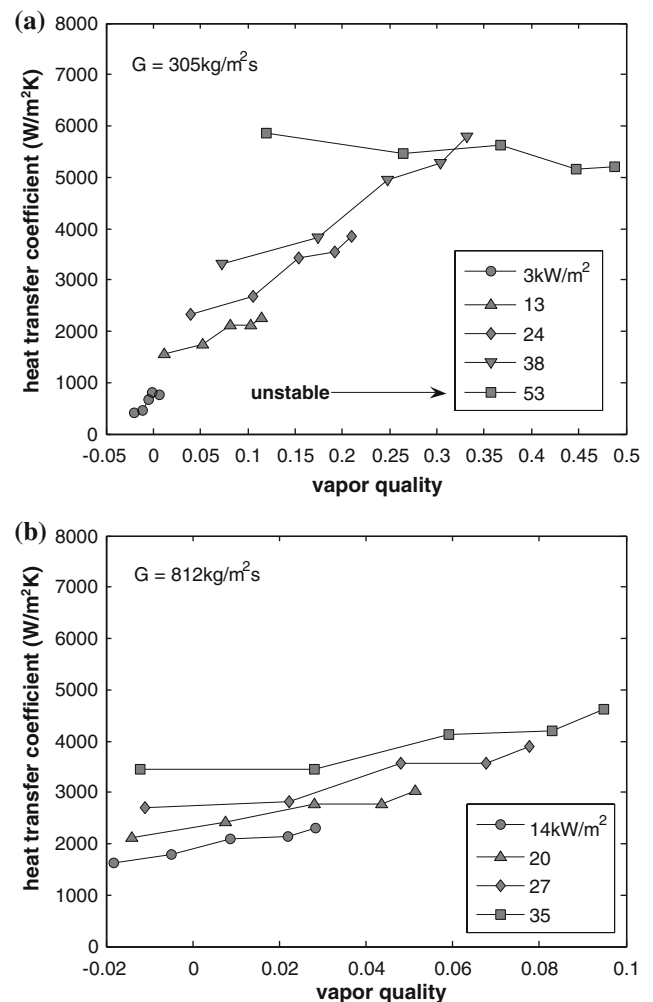
Fig. 14 Experimental heat transfer coefficients versus vapor quality for flow boiling of R-245fa in the 510 μm tube for (**a**) 305 and (**b**) 812 kg/m^2 s. The flow enters the channel as a sub-cooled liquid at 30°C, and exits as a saturated two-phase fluid at 32°C

increased, the second mode dampens, and eventually disappears entirely at 87 kW/m^2. The underlying reasons for the periodic temperatures are (1) the local change in flow temperature associated with the pressure fluctuations due to the bubble growth, expansion, and flushing process, and (2) the cyclical variations in the heat transfer mechanisms. This conclusion is supported by the differences in the measured fluid temperatures at the evaporator exit, also shown in Fig. 19. At 27 kW/m^2 the 7.3 Hz mode present in the temperature of the heated wall vanishes, while at 87 kW/m^2 the fluid temperature behaves irregularly with, however, no dominant frequency.

To assess the differences in the estimated heat transfer coefficients between a stable and an unstable flow, several tests were performed under unstable conditions. Figure 20 compares corresponding heat transfer measurements for four sets of data: one refers to a stable flow of R-245fa, while the remaining three refer to flows exposed to
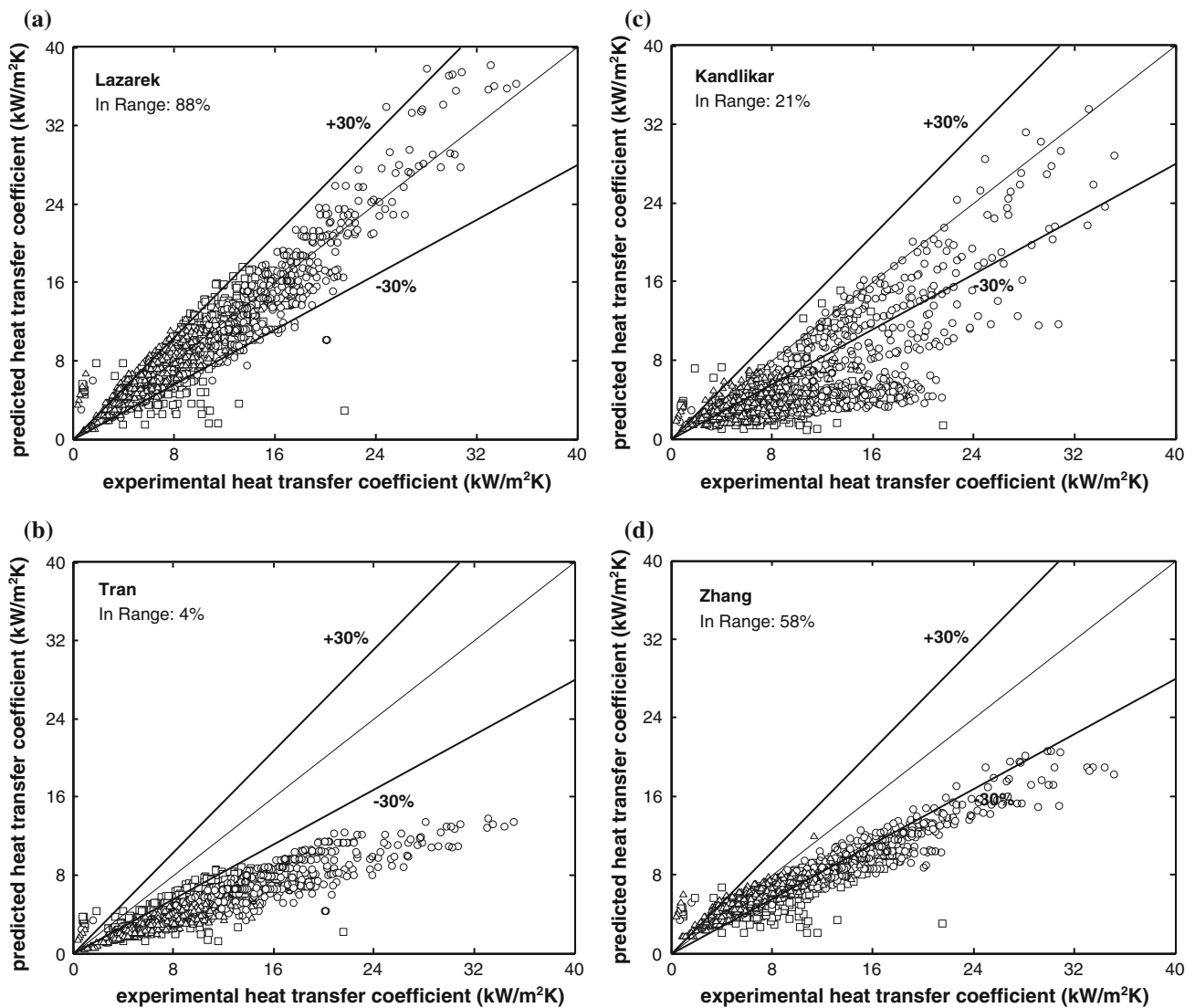
Fig. 15 Predicted versus experimental heat transfer coefficients. The predicted values refer to the methods by Lazarek and Black (1982), Tran et al. (1996), Kandlikar and Balasubramanian (2004), and Zhang et al. (2004). *Circle* R-134a, *square* R-236fa, *triangle* R-245fa

instabilities of different degrees. The data for the unstable cases are computed utilizing time-averaged wall and fluid temperatures (over a 3 s period and a sampling rate of 1,000 samples per second). For the run with mild oscillations (a maximum amplitude in the outer wall temperature of $\Delta T_1 \approx 0.5°C$), the heat transfer coefficients behave as in the case of a stable flow. However, once the flow becomes notably unstable, the outer wall temperature fluctuations reach amplitudes of $\Delta T_1 \approx 4°C$, and their mean values change, delivering completely different trends in the α-x plane. Figure 20 shows an absolute deviation from the stable flow data of 42% at a vapor quality of $x = 0.26$.

Although the largest effect of instability in the heat transfer coefficients occurs for R-245fa, R-236fa also exhibits similar differences with respect to equivalent

stable flow boiling. On the other hand, R-134a requires a very high heat flux for the instabilities to propagate. Figure 21 compares sets of data showing stable versus unstable heat transfer trends for R-236fa and R-134a at a fixed heat flux and mass velocity. For the given operating conditions, the local heat transfer coefficients for R-134a for an unstable flow are essentially identical to those for a stable flow, while for the two low pressure fluids this is not so. This insensitivity to flow instabilities of R-134a points it as being a good working fluid for electronics cooling.

The heat transfer data for flows affected by the oscillatory phenomenon generally show minimal influence of mass velocity, with slightly downward trends with vapor quality in the α-x plane, as was previously noticed in the investigations by Hetsroni et al. (2005) and Xu et al. (2005). The coefficients were often seen to increase with
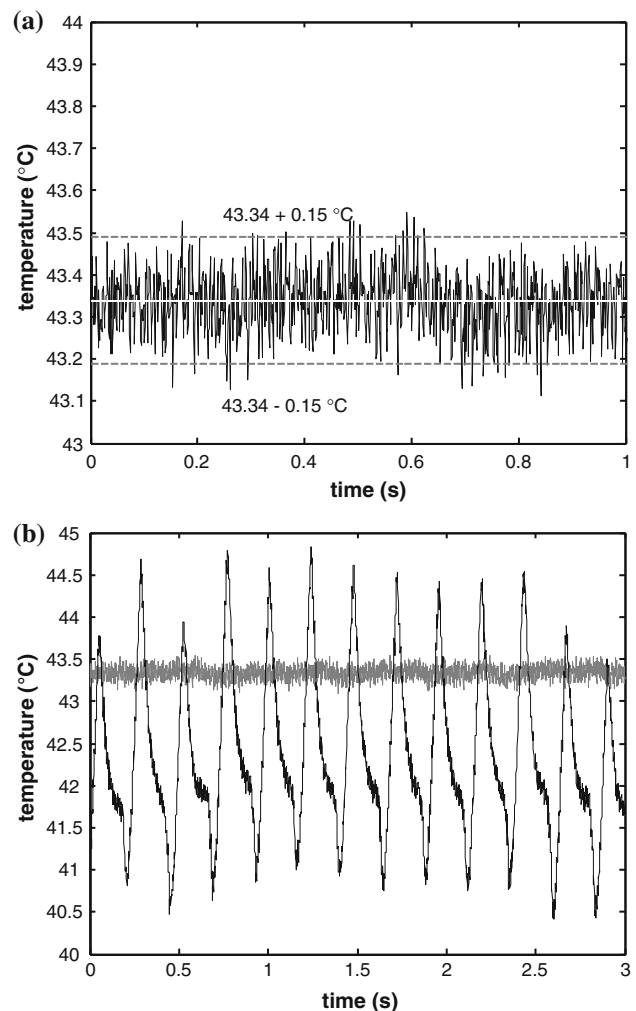
(a)

(b)
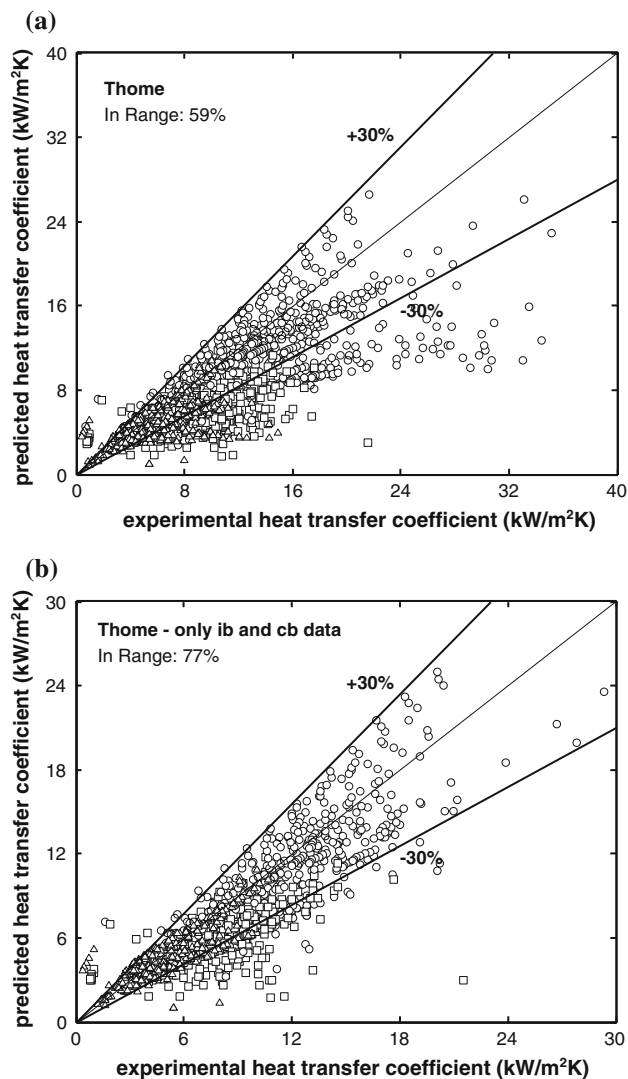
Fig. 16 Three-zone model (Thome et al. 2004) predictions versus the experimental heat transfer coefficients for (**a**) the entire database, and (**b**) only data for isolated bubble and coalescing bubble flows. *Circle* R-134a, *square* R-236fa, *triangle* R-245fa

(a)

(b)

Fig. 17 a Steady outer wall temperature during flow boiling, and **b** wall temperature during flow instability (*black curve*) as compared to the steady profile (shown in *gray*). Values refer to R-245fa in the 510 μm tube, a heat flux of 50 kW/m², and mass velocities of 500 kg/m² s (steady case) and 400 kg/m² s (unstable case)

heat flux, although not in all cases. From some of the data, it appears that for sufficiently high heat fluxes, the heat transfer coefficients become less sensitive to q. The present results show quite conclusively that published data must be segregated into stable and unstable categories to be useful for development of prediction methods.

10 Conclusions

The present experiments on stable two-phase micro-channel flows for the three fluids tested have given clear indications as to the different parameters that govern the heat transfer process. While for R-134a and R-236fa, the heat transfer coefficients have been shown to be strongly dependent on heat flux and fluid properties even up to high vapor qualities

(even when annular flow is the dominant flow mode), the lowest pressure fluid R-245fa has distinguished itself by exhibiting different heat transfer trends. At low vapor qualities, the heat transfer coefficients for R-245fa are heat flux dependent as in the case of the other two fluids. However, at higher vapor qualities, the heat flux dependence disappears, and the curves on the α-x plane increase monotonically with vapor quality rather than decrease or remaining flat. Among the methods for predicting micro-channel heat transfer considered, the Lazarek–Black correlation (Lazarek and Black 1982) gave the best performance, predicting 88% of the database with ±30%.

In contrast to the stable case, a flow affected by an oscillatory instability is exposed to oscillations in local pressure/temperature and heat transfer mechanisms. The global effect on the heated wall is a corresponding temperature oscillation, which combines both of these effects.
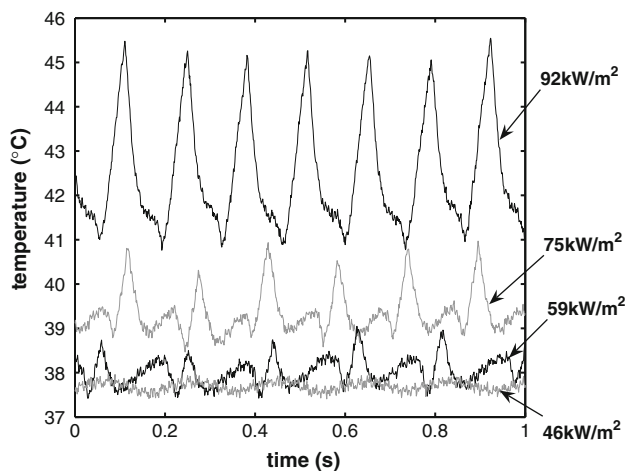
Fig. 18 Wall temperature fluctuations taken 65 mm downstream of the entrance to the evaporator, for an R-236fa flowing with a mass velocity of 700 kg/m^2 s
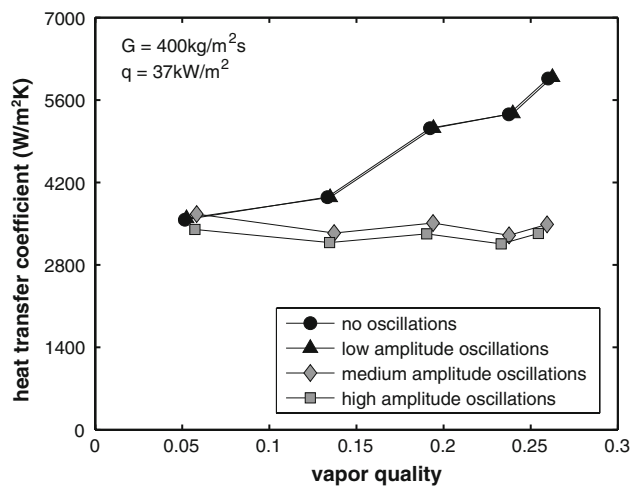
Fig. 20 Stable and unstable heat transfer coefficients for R-245fa with $D = 510$ μm, $T_0 = 30°C$ and $T_L = 32°C$
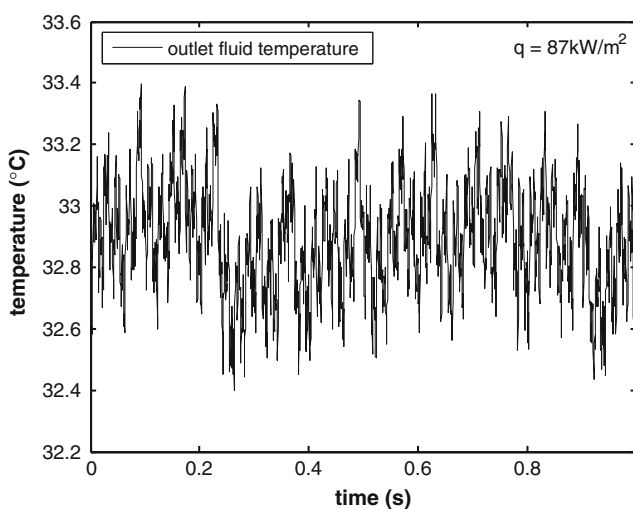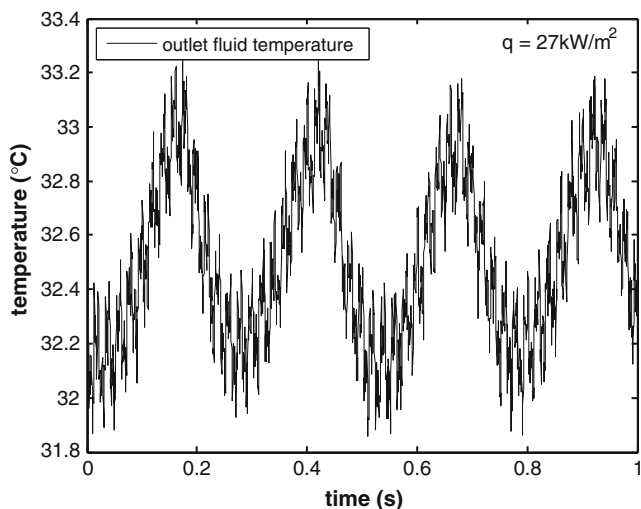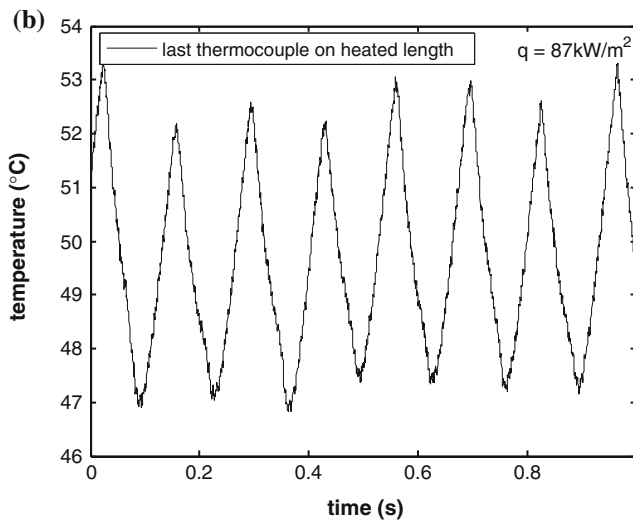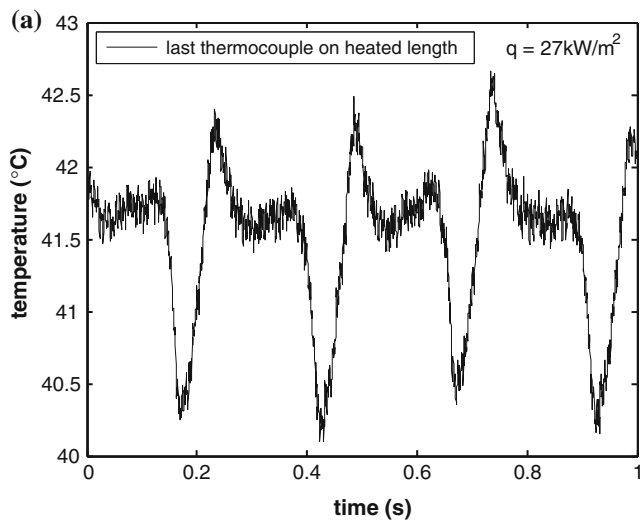
Fig. 19 Wall and fluid temperature fluctuations for unstable flow boiling of R-245fa (510 μm tube) and a mass velocity of 400 kg/m^2 s for (**a**) 27 kW/m^2 and (**b**) 87 kW/m^2
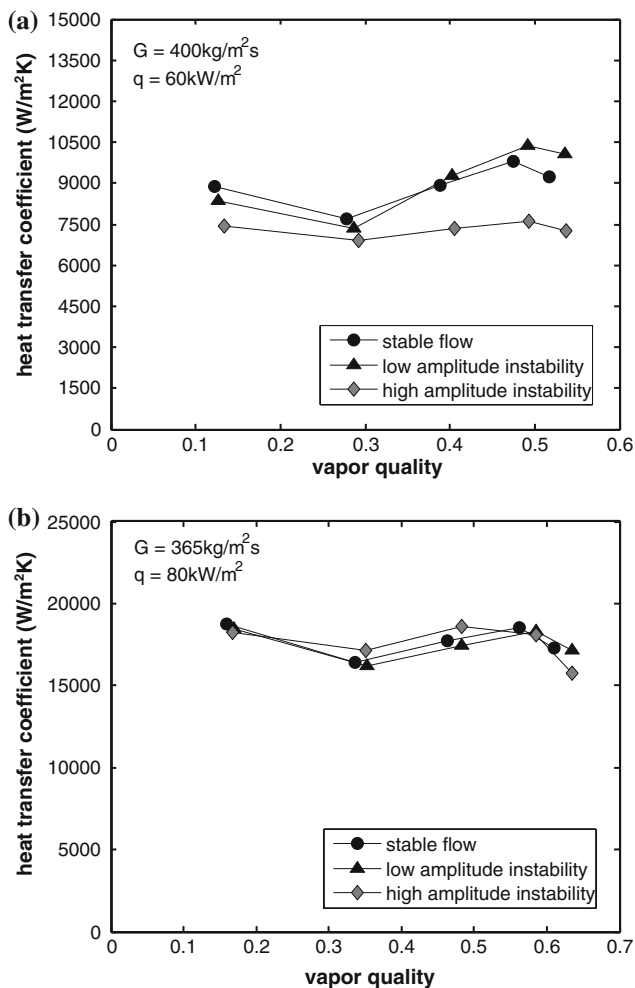
Fig. 21 Heat transfer coefficients computed from stable and unstable flow data for (**a**) R-236fa at 30°C, and (**b**) R-134a at 31°C. $D = 510$ μm in both cases

Assessing local heat transfer coefficients from a flow that is subjected to instability, neglecting the fluctuations, may lead to a substantial deviation from a corresponding stable flow. It is therefore of paramount importance to distinguish between stable and oscillating two-phase flows in the measurement and reporting of flow boiling heat transfer coefficients in micro-channels, to avoid superposing data of two different natures in the development and validation of two-phase heat transfer models and correlations.

References

Agostini B, Thome JR, Fabbri M, Calmi D, Kloter U, Michel B (2008a) High heat flux flow boiling in silicon multi-microchannels: Part I. Heat transfer characteristics of R-236fa. Int J Heat Mass Transf. doi:10.1016/j.ijheatmasstransfer.2008.03.006

Agostini B, Thome JR, Fabbri M, Calmi D, Kloter U, Michel B (2008b) High heat flux flow boiling in silicon multi-microchannels: Part II. Heat transfer characteristics of R-245fa. Int J Heat Mass Transf. doi:10.1016/j.ijheatmasstransfer.2008.03.007

Bao ZY, Fletcher DF, Haynes BS (2000) Flow boiling heat transfer of Freon R11 and HCFC123 in narrow passages. Int J Heat Mass Transf 43:3347–3358

Bergles AE, Kandlikar SG (2005) On the nature of critical heat flux in microchannels. J Heat Transf 127:101–107

Brutin D, Topin F, Tadrist L (2003) Experimental study of unsteady convective boiling heat transfer in heated minichannels. Int J Heat Mass Transf 46:2957–2965

Celata GP (2005) Preface to the special issue dedicated to the ECI international conference on heat transfer and fluid flow in microscale. Experimental thermal and fluid science, Castelvecchio Pascoli, Italy, 25–30 September 2005

Churchill WC, Chu HHS (1975) Correlating equations for laminar and turbulent free convection from a horizontal cylinder. Int J Heat Mass Transf 18:1049–1053

Hetsroni G, Mosyak A, Pogrebnyak E, Segal Z (2005) Explosive boiling of water in parallel micro-channels. Int J Multiph Flow 31:371–392

Kandlikar SG, Balasubramanian P (2004) An extension of the flow boiling correlation to transition, laminar, and deep laminar flows in mini-channels and micro-channels. Heat Transf Eng 25(3):86–93

Kenning DBR, Yan Y (2001) Saturated flow boiling of water in a narrow channel experimental investigation of local phenomena. Trans I Chem 79:425–436

Lazarek GM, Black SH (1982) Evaporative heat transfer, pressure drop and critical heat flux in a small vertical tube with R-113. Int J Heat Mass Transf 25(7):945–960

Lihong W, Min C, Groll M (2005) Experimental study of flow boiling heat transfer in mini-tube. ICMM2005

Lin S, Kew PA, Cornwell K (2001) Two-phase heat transfer to a refrigerant in a 1 mm diameter tube. Int J Refrig 24:51–56

Martín-Callizo C, Ali R, Palm B (2007) New experimental results on flow boiling of R-134a in a vertical microchannel. In: UK heat transfer 2007 proceedings, Edinburgh, 10–11 September 2007

Revellin R, Thome JR (2006) A new type of diabetic flow pattern map for boiling heat transfer in microchannels. J Micromech Microeng 17:788–796

Saitoh S, Daiguji H, Hihara E (2005) Effect of tube diameter on boiling heat transfer of R–134a in horizontal small-diameter tubes. Int J Heat Mass Transf 48:4973–4984

Shiferaw D, Huo X, Karayiannis TG, Kenning DBR (2007) Examination of heat transfer correlations and a model for flow boiling of R–134a in small diameter tubes. Int J Heat Mass Transf 50:5177–5193

Sumith B, Kaminaga F, Matsumura K (2003) Saturated flow boiling of water in a vertical small diameter tube. Exp Thermal Fluid Sci 27:789–801

Thome JR, Dupont V, Jacobi AM (2004) Heat transfer model for evaporation in microchannels. Part I: presentation of the model. Int J Heat Mass Transf 47:3375–3385

Tran TN, Wambsganss MW, France DM (1996) Small circular- and rectangular-channel boiling with two refrigerants. Int J Multiph Flow 22(3):485–498

Xu J, Shen S, Gan Y, Li Y, Zhang W, Su Q (2005) Transient flow pattern based microscale boiling heat transfer mechanisms. J Micromech Microeng 15:1344–1361

Zhang W, Hibiki T, Mishima K (2004) Correlation for flow boiling heat transfer in mini-channels. Int J Heat Mass Transf 47:5749–5763